

Accepted Manuscript

A nonlinear dynamic model of fiber-reinforced composite thin plate with temperature dependence in thermal environment

Hui li, Huaishuai Wu, Tinan Zhang, Bangchun Wen, Zhongwei Guan



PII: S1359-8368(18)31910-3

DOI: <https://doi.org/10.1016/j.compositesb.2018.10.070>

Reference: JCOMB 6149

To appear in: *Composites Part B*

Received Date: 18 June 2018

Revised Date: 22 October 2018

Accepted Date: 24 October 2018

Please cite this article as: li H, Wu H, Zhang T, Wen B, Guan Z, A nonlinear dynamic model of fiber-reinforced composite thin plate with temperature dependence in thermal environment, *Composites Part B* (2018), doi: <https://doi.org/10.1016/j.compositesb.2018.10.070>.

This is a PDF file of an unedited manuscript that has been accepted for publication. As a service to our customers we are providing this early version of the manuscript. The manuscript will undergo copyediting, typesetting, and review of the resulting proof before it is published in its final form. Please note that during the production process errors may be discovered which could affect the content, and all legal disclaimers that apply to the journal pertain.

A nonlinear dynamic model of fiber-reinforced composite thin plate with temperature dependence in thermal environment

Hui li¹⁻², Huaishuai Wu¹, Tinan Zhang¹, Bangchun Wen¹ and Zhongwei Guan²

¹School of Mechanical Engineering and Automation, Northeastern University, Shenyang 110819, China

²School of Engineering, University of Liverpool, Brownlow Street, Liverpool L69 3GQ, United Kingdom

Abstract: In this paper, the material nonlinearity induced by the high temperature is introduced in the modeling of fiber-reinforced composite thin plate structure, and a nonlinear dynamic model in thermal environment is established using Hamilton's principle in conjunction with the classical laminated plate theory, complex modulus method and strain energy method. The nonlinear relationships between the elastic moduli, Poisson's ratios and loss factors and temperature change are expressed by the polynomial method. Then, the dynamic equations in the high temperature environment are derived to solve the inherent characteristics, dynamic responses and damping parameters with considering temperature dependent property. Also, the identification principle of concerned fitting coefficients in the theoretical model is illustrated. As an example to demonstrate the feasibility of the developed model, the experimental test of a TC500 carbon/epoxy composite thin plate is implemented. The results of the developed model and experimental test show a good consistency, and both indicate that the high temperature has complicated influence on its dynamic characteristics, especially on damping property.

Keywords: Nonlinear dynamic model; Fiber-reinforced composite thin plate; Temperature dependent property; Polynomial method; Thermal environment

1. Introduction

The fiber-reinforced composite has excellent mechanical properties, good thermal stability and capability on weight reduction, which is widely used in the aeronautics, astronautics, naval vessel and weapon industry [1-2]. Currently, there are a large number of such composite thin plate structures which are working in thermal environment, such as the composite panels in the high-speed aircraft, the high temperature turbine blades in the aeroengine, and the composite wings in the solar unmanned aircraft. The thermal environment could not only reduce the strength and increase the vibration level of such composite blades and plates, but also bring the deterioration, delamination and fatigue damage to composite structures. Therefore, it is of great scientific significance to study their dynamic characteristics and the corresponding theoretical analysis and modeling methods in the high-temperature environment [3].

Nowadays, some scholars and researchers have carried out a large number of studies on the linear and nonlinear vibration of the fiber-reinforced composite thin plate (FCTP). However, most of them focus on the dynamic problem without considering the temperature effect, with most nonlinear methods being achieved by

the Von Kármán nonlinear strain-displacement relationships. Rao and Pillai [4] analyzed the large-amplitude vibrations of a simply supported composite plate with immovable edges. The Kirchhoff's hypothesis and the strain-displacement relationships of von Kármán type were used in the formulation with the in-plane deformation and inertias being considered. Singh et al. [5] presented a direct numerical integration method of the frequency/time period expression to study the nonlinear vibration behavior of the fiber-reinforced plates. Ribeiro and Petyt [6] studied the geometrically nonlinear vibration of a thin laminated composite plate under the fully clamped boundary condition by the hierarchical finite element with consideration of Von Kármán nonlinear assumption. Chen et al. [7] presented the semi-analytical finite strip method to analyze the geometrically nonlinear response of a rectangular composite laminated plate under the simply supported boundary condition with the von Karman assumptions. Singha and Daripa [8] used the shear deformable finite element method to analyze the large-amplitude vibration characteristics of the composite plates under the transverse harmonic pressure.

Some studies were also reported on the linear dynamic analysis and modelling of the composite plate

structures in thermal environment. Whitney et al. [9] studied the buckling and elastic response of the composite plates under thermal condition with the classical laminated plate theory. Ram and Sinha [10] established finite element model of the laminated composite plates in hygrothermal environment and solved the non-dimensional natural frequencies under simply supported and clamped boundary conditions. Gilat et al. [11] investigated the dynamic inelastic response and buckling of a metal matrix reinforced laminated composite plate under the effect of the thermo-mechanical coupling by the finite difference spatial domain method and Runge–Kutta method. Matsunaga [12] presented a two-dimensional global higher-order deformation theory to solve natural frequencies and critical temperatures of the simply supported multilayered plates subjected to thermal loading. Li and Li [13] investigated the effects of thermal environments on the vibration and sound radiation characteristics of an asymmetric laminated plate, and obtained the natural frequencies, resonant amplitudes and sound pressure levels base on the FEM and the BEM.

In addition, several experimental studies in thermal environment on the dynamic characteristics of the fiber-reinforced composite plates were also reported. Melo and Radford [14] measured the time and temperature dependence of the viscoelastic properties of the composite plate using dynamic mechanical analysis equipment. The results showed that a decrease in the storage moduli and an increase in loss factors as temperature increased. Also, the measured changes in loss factors with the temperature between 20 °C and 120 °C were much larger than changes in storage moduli. Yang et al. [15] experimentally investigated the effect of the varying thermal conditions on the modal parameters of the composite laminate plate by the stochastic subspace identification method. It was found that the frequencies and damping ratios had strong negative correlation with temperature, but no clear correlation of modal shapes with temperature changes could be observed. Sefrani et al. [16] experimentally studied the temperature effect on the bending modulus and damping of the glass fiber composite beam. The results showed that the dynamic properties were appreciably kept up to the temperature of glass transition, where damping increased sharply in a little interval of temperature. Wu et al. [17] established a thermal/vibration test system of composite plates at

1200 °C, where a self-developed extension configuration of a high-temperature resistant ceramic pole was used to transfer the vibration signals of the structure to a non-high temperature zone.

As this paper focuses on the nonlinear dynamic modelling and analysis method of the composite structures in thermal environment, some important and selective literatures on this topic were highlighted here. Praveen and Reddy [18] analyzed the geometrically nonlinear static and dynamic response of the functionally graded plates subjected to the temperature loads based on the von Karman theory. Duc et al. [19–23] conducted a series of nonlinear mechanical, vibration and buckling analysis of the functionally graded circular, conical and elliptical cylindrical shells in thermal environment with and without considering the elastic foundations. The von Karman nonlinearity, Galerkin method, fourth order Runge–Kutta method, etc. were employed to calculate natural frequencies, nonlinear frequency–amplitude relation and dynamic response of the shells, and the nonlinear relationship between material properties and thermal load were also discussed. Wang et al. [24] investigated the nonlinear large-amplitude responses of a functionally graded material plate by considering the thermal effect and the longitudinal velocity based on the D'Alembert's principle. Gao et al. [25] established the nonlinear dynamic response equations of composite orthotropic plate under thermal environment. The Galerkin method and Airy's stress function are implemented to obtain the natural frequency, frequency-amplitude curve and nonlinear dynamic responses. Thanh et al. [26] studied the nonlinear dynamic response and vibration of functionally graded carbon nanotube-reinforced composite cylindrical shell in thermal environment. The influences of temperature-dependent material properties on the nonlinear vibration were also analyzed.

Up to date, it is clear that the research on nonlinear dynamic modelling techniques is still limited for the analysis of fiber-reinforced composite thin plates in thermal environment, especially less attention being paid to the damping modelling in the high temperature environment. Besides, most of research studies focus the geometric nonlinearity of the composite plates based on the Von Kármán strain-displacement relationships, which are in lack of the experimental verification in thermal environment. Therefore, it is still necessary to put efforts

to study the nonlinear dynamic problems of such composite plate structures, especially to establish an appropriate mathematical model to describe the nonlinear dynamic phenomenon with temperature dependence.

2. Establishment of the nonlinear dynamic model of FCTP in thermal environment

2.1 A nonlinear dynamic model of FCTP in thermal environment

Assume that a fiber-reinforced composite thin plate, which is made of the fiber and matrix material with n layers, is under a uniform thermal environment, as seen in Fig.1. Firstly, set up the coordinate system xOy at the middle surface, and suppose the length, width and thickness are expressed as a , b and h , and the fiber direction within a layer is defined as θ from the x -axis of the coordinate system. In this theoretical model, each layer of the composite plate is located at h_{k-1} and h_k along the z -axis with the equal thickness, "1" represents the direction parallel to the fiber, "2" represents the direction perpendicular to the fiber and "3" represents the direction perpendicular to the 1-2 surface. In addition, the plate is under cantilever boundary condition, which is subjected to the pulse excitation force $F(t)$ in the point $R_e(x_0, y_0)$, $w(t)$ is the vibration displacement in any point $R_r(x_1, y_1)$, ρ is the density, and α_1 , α_2 are the thermal expansion coefficients parallel and perpendicular to the fiber direction.

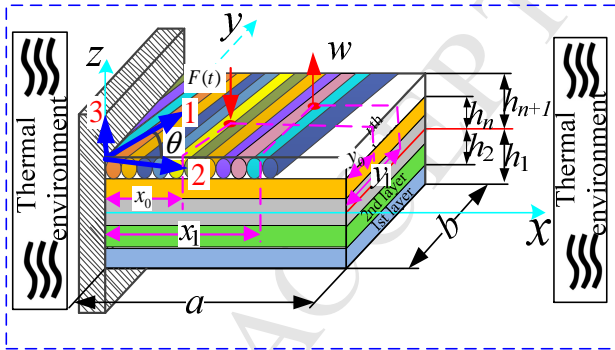


Fig. 1 Theoretical model of FCTP in thermal environment

Considering the influence of the high temperature environment on the fiber-reinforced material parameters, the polynomial method can be employed to establish the nonlinear relationships between the material parameters of fiber composite and temperature change value in different fiber directions [27, 28].

$$\begin{aligned} E_1'(\Delta T) &= E_1^0 + A_1(\Delta T) + A_2(\Delta T)^2 + A_3(\Delta T)^3 + \dots + A_{n_0}(\Delta T)^{n_0} \\ E_2'(\Delta T) &= E_2^0 + B_1(\Delta T) + B_2(\Delta T)^2 + B_3(\Delta T)^3 + \dots + B_{n_0}(\Delta T)^{n_0} \\ G_{12}'(\Delta T) &= G_{12}^0 + C_1(\Delta T) + C_2(\Delta T)^2 + C_3(\Delta T)^3 + \dots + C_{n_0}(\Delta T)^{n_0} \\ v_{12}'(\Delta T) &= v_{12}^0 + D_1(\Delta T) + D_2(\Delta T)^2 + D_3(\Delta T)^3 + \dots + D_{n_0}(\Delta T)^{n_0} \\ \eta_1'(\Delta T) &= \eta_1^0 + F_1(\Delta T) + F_2(\Delta T)^2 + F_3(\Delta T)^3 + \dots + F_{n_0}(\Delta T)^{n_0} \end{aligned}$$

$$\begin{aligned} \eta_2'(\Delta T) &= \eta_2^0 + H_1(\Delta T) + H_2(\Delta T)^2 + H_3(\Delta T)^3 + \dots + H_{n_0}(\Delta T)^{n_0} \\ \eta_{12}'(\Delta T) &= \eta_{12}^0 + P_1(\Delta T) + P_2(\Delta T)^2 + P_3(\Delta T)^3 + \dots + P_{n_0}(\Delta T)^{n_0} \end{aligned} \quad (1)$$

where $E_1^0, E_2^0, G_{12}^0, v_{12}^0, \eta_1^0, \eta_2^0, \eta_{12}^0$ represent elastic moduli, Poisson's ratios and loss factors of the composite thin plate under normal temperature, $A_{n_0}, B_{n_0}, C_{n_0}, D_{n_0}, F_{n_0}, H_{n_0}, P_{n_0}$ are the fitting coefficients of the composite thin plate in all directions of the fiber when the high temperature environment is considered, n_0 is the maximum of the polynomial order, and ΔT is the temperature change relative to the normal temperature environment.

Then, consider the influence of different fiber directions, the elastic modulus of the composite thin plate can be expressed as

$$\begin{aligned} E_1^*(\Delta T) &= E_1'(\Delta T)(1 + i\eta_1') \\ E_2^*(\Delta T) &= E_2'(\Delta T)(1 + i\eta_2') \\ G_{12}^*(\Delta T) &= G_{12}'(\Delta T)(1 + i\eta_{12}') \end{aligned} \quad (2)$$

where E_1^*, E_2^* represents the complex moduli paralleled and perpendicular to the fiber in thermal environment, respectively, G_{12}^* represents the complex shear modulus in the 1-2 surface, and E_1', E_2', G_{12}' represents the real part of complex moduli E_1^*, E_2^*, G_{12}^* in thermal environment, respectively.

By referring to the literature [9], the generalized Duhamel-Neumann form of Hooke's law for the relationship of the stress and strain in thermal environment can be expressed as

$$\varepsilon_i = S_{ij}\sigma_j + \bar{\varepsilon}_i \quad (i, j = 1, 2, 6) \quad (3)$$

where, the stresses are denoted by $\sigma_1 = \sigma_x, \sigma_2 = \sigma_y, \sigma_6 = \sigma_{xy}$, the strains are denoted by ε_i , and the thermal expansion strains are denoted by $\bar{\varepsilon}_i$.

The inverted form of the Eq. (3) is

$$\sigma_i = \bar{Q}_{ij}(\varepsilon_j - \bar{\varepsilon}_j) \quad (i, j = 1, 2, 6) \quad (4)$$

where \bar{Q}_{ij} is the stiffness matrix, it contains the following matrix elements

$$\begin{aligned}
\bar{Q}_{11} &= Q_{11} \cos^4 \theta_k + 2(Q_{12} + 2Q_{66}) \sin^2 \theta_k \cos^2 \theta_k + Q_{22} \sin^4 \theta_k \\
\bar{Q}_{12} &= (Q_{11} + Q_{22} - 4Q_{66}) \sin^2 \theta_k \cos^2 \theta_k + Q_{12} (\sin^4 \theta_k + \cos^4 \theta_k) \\
\bar{Q}_{22} &= Q_{11} \sin^4 \theta_k + 2(Q_{12} + 2Q_{66}) \sin^2 \theta_k \cos^2 \theta_k + Q_{22} \cos^4 \theta_k \\
\bar{Q}_{16} &= (Q_{11} - Q_{12} - 2Q_{66}) \sin \theta_k \cos^3 \theta_k \\
&\quad + (Q_{12} - Q_{22} + 2Q_{66}) \sin^3 \theta_k \cos \theta_k \\
\bar{Q}_{26} &= (Q_{11} - Q_{12} - 2Q_{66}) \sin^3 \theta_k \cos \theta_k \\
&\quad + (Q_{12} - Q_{22} + 2Q_{66}) \sin \theta_k \cos^3 \theta_k \\
\bar{Q}_{66} &= (Q_{11} + Q_{22} - 2Q_{12} - 2Q_{66}) \sin^2 \theta_k \cos^2 \theta_k \\
&\quad + Q_{66} (\sin^4 \theta_k + \cos^4 \theta_k) \\
Q_{11} &= \frac{E_1^*}{1 - \nu_{12}\nu_{21}}, \quad Q_{12} = \frac{\nu_{12}E_2^*}{1 - \nu_{12}\nu_{21}} \\
Q_{22} &= \frac{E_2^*}{1 - \nu_{12}\nu_{21}}, \quad Q_{66} = G_{12}^*, \quad \nu_{21} = \nu_{12} \frac{E_2^*}{E_1^*} \quad (5)
\end{aligned}$$

Since \bar{Q}_{ij} consists of the real and imaginary part, it can be expressed as the following form

$$\bar{Q}_{ij} = \bar{Q}'_{ij} + j\bar{Q}''_{ij} \quad (6)$$

where \bar{Q}'_{ij} and \bar{Q}''_{ij} are the real and imaginary parts of the complex stiffness matrix coefficients.

According to the assumption of the laminated plate theory, the total strain of FCTP is

$$\varepsilon_i = \varepsilon_i^0(x, y, t) + zk_i(x, y, t) \quad (i=1, 2, 6) \quad (7)$$

where t denotes the time, ε_i^0 are the mid-plane strains, and k_i are the plate curvatures.

The plate force N_i and moment resultants M_i are defined in the usual manner, i.e.

$$(N_i, M_i) = \int_{-h/2}^{h/2} \sigma_i(1, z) dz \quad (i=1, 2, 6) \quad (8)$$

Substitution of Eq. (7) into Eq. (4) and taking Eq. (8) into account, leads to plate constitutive relations in thermal environment

$$\begin{aligned}
N_i &= A_{ij}\varepsilon_j^0 + B_{ij}k_j - \bar{N}_i \\
M_i &= B_{ij}\varepsilon_j^0 + D_{ij}k_j - \bar{M}_i \quad (i=1, 2, 6) \quad (9)
\end{aligned}$$

where

$$\begin{aligned}
(A_{ij}, B_{ij}, D_{ij}) &= \int_{-h/2}^{h/2} \bar{Q}_{ij}(1, z, z^2) dz \\
(\bar{N}_i, \bar{M}_i) &= \int_{-h/2}^{h/2} \bar{Q}_{ij} \bar{\varepsilon}_j(1, z) dz \quad (10)
\end{aligned}$$

where, \bar{N}_i and \bar{M}_i are the thermal internal force and the thermal moment. It should be noted that for the general case $\bar{\varepsilon}_i = \bar{\varepsilon}_i(x, y, z, t, T)$, where T is the temperature value in the corresponding thermal environment, and for the uniform temperature, the thermal expansion strain is

$$\bar{\varepsilon}_i = \begin{Bmatrix} \alpha_x \\ \alpha_y \\ \alpha_{xy} \end{Bmatrix} \Delta T \quad (i=1, 2, 6) \quad (11)$$

where α_x , α_y , α_{xy} , are the coefficients of thermal expansion along the x , y and shear directions, respectively.

From the classical laminated plate theory

$$\varepsilon^0 = \begin{Bmatrix} \frac{\partial u^0}{\partial x} \\ \frac{\partial v^0}{\partial y} \\ \frac{\partial u^0}{\partial y} + \frac{\partial v^0}{\partial x} \end{Bmatrix}, \quad k = - \begin{Bmatrix} \frac{\partial^2 w}{\partial x^2} \\ \frac{\partial^2 w}{\partial y^2} \\ 2 \frac{\partial^2 w}{\partial x \partial y} \end{Bmatrix} \quad (12)$$

where, u^0 and v^0 are mid-plane displacements in the x , y directions, respectively, and w is the displacement in the z direction.

By referring to the dynamic equations in the literature [9], the equation of vibration displacement of FCTP in thermal environment can be deduced and expressed as

$$\begin{aligned}
L_1 u^0 + 2A_{16} \frac{\partial^2 u^0}{\partial x \partial y} + L_2 v^0 - L_4 \frac{\partial w}{\partial x} - L_5 \frac{\partial w}{\partial y} \\
- \frac{\partial \bar{N}_x}{\partial x} - \frac{\partial \bar{N}_{xy}}{\partial y} = R \frac{\partial^2 u^0}{\partial t^2} \\
L_2 u^0 + L_3 v^0 + 2A_{26} \frac{\partial^2 v^0}{\partial x \partial y} - L_6 \frac{\partial w}{\partial x} - L_7 \frac{\partial w}{\partial y} \\
- \frac{\partial \bar{N}_{xy}}{\partial x} - \frac{\partial \bar{N}_y}{\partial y} = R \frac{\partial^2 v^0}{\partial t^2} \\
4D_{16} \frac{\partial^4 w}{\partial x^3 \partial y} + 4D_{26} \frac{\partial^4 w}{\partial x \partial y^3} + D_{22} \frac{\partial^4 w}{\partial y^4} - L_4 \frac{\partial u^0}{\partial x} - L_5 \frac{\partial u^0}{\partial y} \\
- L_6 \frac{\partial v^0}{\partial x} - L_7 \frac{\partial v^0}{\partial y} + L_8 \frac{\partial^2 w}{\partial x^2} + \frac{\partial^2 \bar{M}_x}{\partial x^2} + 2 \frac{\partial^2 \bar{M}_{xy}}{\partial x \partial y} + \frac{\partial^2 \bar{M}_y}{\partial y^2} \\
+ R \frac{\partial^2 w}{\partial t^2} = q(t) - \bar{N}_x \frac{\partial^2 w}{\partial x^2} - 2\bar{N}_{xy} \frac{\partial^2 w}{\partial x \partial y} - \bar{N}_y \frac{\partial^2 w}{\partial y^2} \quad (13)
\end{aligned}$$

where R is the integral of mass density through the plate thickness, L_i are the operators, $q(t)$ is a distributed pressure over the surface of the composite plate.

Because the concerned composite plate is a symmetric laminated structure, there is no coupling between the tensile and bending loads. The in-plane displacement and surface displacement is decoupled. Then, according to the small deflection theory of the thin composite plate, the principle of minimum potential energy and the Ritz method are combined to solve the

strain energy U_{Nor}

$$U_{Nor} = \frac{1}{2} \int_A \left\{ D_{11} \left(\frac{\partial^2 w}{\partial x^2} \right)^2 + 2D_{12} \frac{\partial^2 w}{\partial x^2} \frac{\partial^2 w}{\partial y^2} + D_{22} \left(\frac{\partial^2 w}{\partial y^2} \right)^2 + 4D_{16} \frac{\partial^2 w}{\partial x \partial y} \frac{\partial^2 w}{\partial x^2} + 4D_{26} \frac{\partial^2 w}{\partial x \partial y} \frac{\partial^2 w}{\partial y^2} + 4D_{66} \left(\frac{\partial^2 w}{\partial x \partial y} \right)^2 \right\} dA \quad (14)$$

where A represents the area of the composite thin plate.

Considering the influence of the thermal environment, the potential energy V_{Tem} of the system induced by the thermal internal force can be expressed as

$$V_{Tem} = \frac{1}{2} \int_A \left(\bar{N}_x \left(\frac{\partial w}{\partial x} \right)^2 + \bar{N}_y \left(\frac{\partial w}{\partial y} \right)^2 + 2\bar{N}_{xy} \frac{\partial w}{\partial x} \frac{\partial w}{\partial y} \right) dA \quad (15)$$

The kinetic energy T_v of the system in thermal environment can be expressed as

$$T_v = \frac{1}{2} \rho h \omega^2 \int_A w^2 dA \quad (16)$$

where ω represents the excitation circular frequency.

2.2 Solutions to the inherent characteristics in thermal environment

Furthermore, the vibration displacement $w(x, y, t)$ of the composite thin plate in thermal environment is assumed to be

$$w(x, y, t) = W(x, y) e^{i\omega t} \quad (17)$$

where, $W(x, y)$ represents the modal shape function which can be defined as

$$W(x, y) = \sum_{m=1}^M \sum_{n=1}^N a_{mn} X_m(x) Y_n(y) \quad (18)$$

where m and n represent the half wavenumber of the modal shapes along x and y directions respectively, M and N are the maximum values of m and n , and a_{mn} is the coefficient. Besides, $X_m(x)$ and $Y_n(y)$ are the modal functions along x and y directions respectively, which can be expressed by the fixed-free beam function and free-free beam function.

Then, according to the Ritz method and neglecting the influence of the harmonic component $e^{i\omega t}$, the Lagrange energy function Π can be defined as

$$\Pi = U_{Nor} + V_{Tem} - T_v \quad (19)$$

By minimizing the partial derivative of the Lagrange energy function Π with the respect to a_{mn} in the following equation

$$\frac{\partial \Pi}{\partial a_{mn}} = 0, m = 1, 2, \dots, M, n = 1, 2, \dots, N \quad (20)$$

By substituting Eqs. (14), (15) and (16) into Eq. (20),

the following equation can be obtained

$$(\mathbf{K} - \omega^2 \mathbf{M}) \mathbf{a} = 0 \quad (21)$$

where \mathbf{K} and \mathbf{M} represent the stiffness matrix and mass matrix of the system, respectively, and $\mathbf{a} = (a_{11}, a_{12}, \dots, a_{mn})^T$ is the eigenvector.

By solving Eq. (21), the natural frequencies of FCTP in the high temperature environment can be obtained. Then, by substituting the eigenvector $\mathbf{a} = (a_{11}, a_{12}, \dots, a_{mn})^T$ related with the certain natural frequency into Eq. (18), the corresponding modal shape can be obtained. Repeating these steps above, all the concerned modal shapes can be obtained.

2.3 Solutions to the dynamic response in thermal environment

After the natural frequencies and modal shapes of FCTP are solved, assume that the pulse excitation $F(t)$ is exerted on the point $R_e(x_0, y_0)$, which is perpendicular to the plate surface. $F(t)$ can be described by Dirac function as

$$F(t) = f(t) \delta(x - x_0) \delta(y - y_0) \quad (22)$$

$$f(t) = \begin{cases} f_0 \sin(\omega t), & 0 \leq t \leq t_1 \\ 0, & t > t_1 \end{cases}$$

where ω is excitation circular frequency, t_1 is excitation time.

On the basic of the mode superposition principle, the dynamic responses $w(t)$ can be expanded in terms of the mode functions as follows

$$w(t) = \sum_{m=1}^{\infty} \sum_{n=1}^{\infty} W_{mn}(x, y) T_{mn}(t) \quad (23)$$

where, $W_{mn}(x, y)$ is modal shape function, T_{mn} is modal component.

Substituting the dynamic response $w(t)$ and the modal shape function W_{mn} into Eq. (13), the following equation can be derived after the simplification

$$\sum_{m=1}^{\infty} \sum_{n=1}^{\infty} \left(\rho h \frac{d^2 T_{mn}}{dt^2} + \rho h (\omega)^2 T_{mn} \right) W_{mn} = F \quad (24)$$

Then, multiply $W_{kl}(x, y)$ ($k, l = 1, 2, 3, \dots$) at both sides of Eq. (24) and perform the integral operation along the x - y surface, the following equation can be obtained

$$\sum_{m=1}^{\infty} \sum_{n=1}^{\infty} \iint_A \left(\rho h \frac{d^2 T_{mn}}{dt^2} + \rho h (\omega)^2 T_{mn} \right) W_{mn} W_{kl} dA = \iint_A F W_{kl} dA \quad (25)$$

Further, by using the orthogonality of modal shape of the plate with the following form

$$\iint_A \rho h W_{mn} W_{kl} dA = 0 \quad (m \neq k \text{ or } n \neq l) \quad (26)$$

The generalized vibration differential equation without damping can be expressed as

$$\frac{d^2 T_{mn}(t)}{dt^2} + (\omega)^2 T_{mn}(t) = \frac{P_{mn}(t)}{M_{mn}} \quad (27)$$

where $P_{mn}(t)$ and M_{mn} are the generalized force and generalized mass, respectively, which have the following form

$$P_{mn}(t) = f(t) W_{mn}(x_1, y_1)$$

$$M_{mn} = \iint_A \rho h (W_{mn}(x, y))^2 dA \quad (28)$$

Similarly, under the assumption of the small damping, the generalized vibration differential equation with damping can be expressed as

$$\frac{d^2 T_{mn}(t)}{dt^2} + 2\zeta_r \omega \frac{dT_{mn}}{dt} + (\omega)^2 T_{mn}(t) = \frac{P_{mn}(t)}{M_{mn}} \quad (29)$$

where ζ_r is the modal damping ratio at the r mode of the composite plate.

At the zero-initial condition, the solution of Eq. (29) can be expressed as Duhamel integral form, which has the following expression

$$T_{mn}(t) = \frac{W_{mn}(x_1, y_1)}{\omega_d M_{mn}} \int_0^t f(\tau) e^{-\zeta_r \omega(t-\tau)} \sin \omega_d(t-\tau) d\tau \quad (30)$$

where ω_d is the circular frequency of the damped system, which can be expressed as $\omega_d = \sqrt{1 - \zeta_r^2} \omega$

Eq. (30) can be solved using Simpson numerical integration technique, and by substituting the results into Eq. (23), the dynamic response $w(t)$ of the composite thin plate under the pulse excitation can be obtained by the modal shape superposition method.

$$w(t) = \sum_{m=1}^{\infty} \sum_{n=1}^{\infty} W_{mn}(x, y) T_{mn}(t) \quad (31)$$

2.4 Solutions to the damping in thermal environment

Based on the strain energy method, the total strain energy U of FCTP in thermal environment can be expressed as

$$U = U_x + U_y + U_{xy} + U_{\text{Tem}} \quad (32)$$

where, U_x , U_y , U_{xy} represent the strain energy along the x , y , and xy directions respectively, and U_{Tem} is the potential energy induced by the thermal internal forces

$$U_x = \frac{1}{2} \sum_{k=1}^n \int_{x=0}^a \int_{y=0}^b \int_{h_{k-1}}^{h_k} \sigma'_x \varepsilon_x dx dy dz$$

$$U_y = \frac{1}{2} \sum_{k=1}^n \int_{x=0}^a \int_{y=0}^b \int_{h_{k-1}}^{h_k} \sigma'_y \varepsilon_y dx dy dz$$

$$U_{xy} = \frac{1}{2} \sum_{k=1}^n \int_{x=0}^a \int_{y=0}^b \int_{h_{k-1}}^{h_k} \sigma'_{xy} \gamma_{xy} dx dy dz$$

$$U_{\text{Tem}} = \frac{1}{2} \int_A \left(\overline{N}'_x \left(\frac{\partial w}{\partial x} \right)^2 + \overline{N}'_y \left(\frac{\partial w}{\partial y} \right)^2 + 2\overline{N}'_{xy} \frac{\partial w}{\partial x} \frac{\partial w}{\partial y} \right) dA$$

where, $\sigma'_x, \sigma'_y, \sigma'_{xy}, \overline{N}'_x, \overline{N}'_y, \overline{N}'_{xy}$ can be obtained by solving the real part of complex stiffness matrix coefficients \overline{Q}'_{ij} in Eqs. (4), (6) and (10).

The total dissipated energy of FCTP in thermal environment can be expressed as

$$\Delta U = \Delta U_x + \Delta U_y + \Delta U_{xy} + \Delta U_{\text{Tem}} \quad (33)$$

where

$$\Delta U_x = \pi \sum_{k=1}^n \int_{x=0}^a \int_{y=0}^b \int_{h_{k-1}}^{h_k} \sigma''_x \varepsilon_x dx dy dz$$

$$\Delta U_y = \pi \sum_{k=1}^n \int_{x=0}^a \int_{y=0}^b \int_{h_{k-1}}^{h_k} \sigma''_y \varepsilon_y dx dy dz$$

$$\Delta U_{xy} = \pi \sum_{k=1}^n \int_{x=0}^a \int_{y=0}^b \int_{h_{k-1}}^{h_k} \sigma''_{xy} \gamma_{xy} dx dy dz$$

$$\Delta U_{\text{Tem}} = \pi \int_A \left(\overline{N}''_x \left(\frac{\partial w}{\partial x} \right)^2 + \overline{N}''_y \left(\frac{\partial w}{\partial y} \right)^2 + 2\overline{N}''_{xy} \frac{\partial w}{\partial x} \frac{\partial w}{\partial y} \right) dA$$

where ΔU_x , ΔU_y , ΔU_{xy} represent the dissipated energy along the x , y , and x - y directions respectively, and ΔU_{Tem} is the dissipated energy induced by the thermal internal forces. Besides, $\sigma''_x, \sigma''_y, \sigma''_{xy}, \overline{N}''_x, \overline{N}''_y, \overline{N}''_{xy}$ can be obtained by solving the imaginary part of complex stiffness matrix coefficients \overline{Q}''_{ij} in Eqs. (4), (6) and (10).

Then, the damping ratio of FCTP can be obtained as follow

$$\zeta_r = \frac{\Delta U}{4\pi U} \quad (34)$$

3. Determination of fitting coefficients of the fiber-reinforced composite in thermal environment

3.1 Measurements of the frequency response function (FRF) in thermal environment

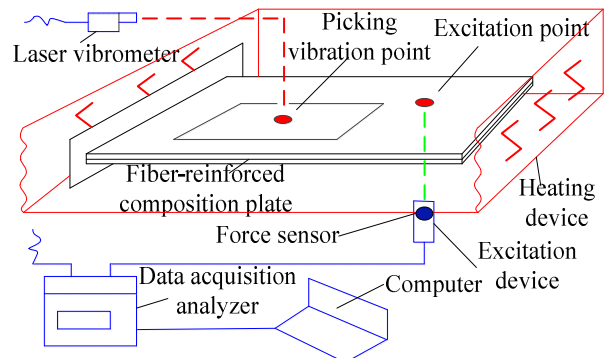


Fig.2 Schematic of FRF measurement of FCTP in thermal environment

In most cases, the hammer excitation is the best choice to measure the FRFs of the plate structures in experiment. Yet in the thermal environment it is difficult for us to hold the hammer. Also, for the sake of the safety of the instrument and operator, an alternative excitation method needs to be considered. Assuming that the pulse excitation of force sensor driven by the aerodynamic load can be realized in the real test, and the dynamic response of FCTP can be measured by the laser Doppler vibrometer, then we can use the data acquisition instrument to record the pulse excitation signal of the force sensor and the laser response signal. In this way, the goal of the FRF measurement under high temperature environment can be turned into reality, whose schematic can be seen in the Fig. 2 (the detailed experimental work will be introduced in the case study).

3.2 Identification principle of composite material parameters in thermal environment

Because at the beginning we don't know the nonlinear relationship between temperature and material parameters. In order to determine the assumed fitting coefficients in this nonlinear model, the influence of temperature change ΔT on the material parameters in Eq. (1) is temporarily neglected. In this way, the theoretical FRF can be sequentially obtained, and the concerned material parameters of fiber composite in different thermal environments can also be identified in the iterative calculation process.

In order to calculate the theoretical FRF, the same amplitude of excitation force $F(t)$ with the experiment in time domain is simulated, and then the dynamic response signal $X(t)$ in any point of FCTP can be calculated by the self-written MATLAB program. Consequently, do the Fast Fourier transformation (FFT) operation to the excitation and response signal, the original signal of $F(t)$ and $X(t)$ can be transformed as the Fourier function $F(\omega)$ and $X(\omega)$. According to the definition of frequency response function, the theoretical FRF $H(\omega)$ can be expressed as

$$H(\omega) = \frac{X(\omega)}{F(\omega)} \quad (35)$$

As the measured FRFs of FCTP under different temperature conditions are already obtained (in Section 3.1), we can compare the theoretical FRF with the measured FRF under certain thermal condition. If they are very close to each other, the composite material

parameters of fiber composite, such as elastic moduli, Poisson's ratios and loss factors, can be iteratively obtained by the FRF approximation method (its identification principle will be introduced later). It should be noted that the accuracy of these determined material parameters at certain temperature condition has nothing to do with the above ignorance. As long as the theoretical FRF data and experimental FRF data are close, the calculated material parameters can represent the actual material parameters, which already reflect the influence of certain high temperature on the fiber material.

The identification principle of FRF approximation method is simple yet useful. Fig. 3 gives the corresponding identification schematic of material parameters of fiber-reinforced composite in thermal environment. Firstly, the experimental FRF and theoretical FRF with the two methods described in the above are obtained and plotted on the same graph as shown in Fig. 3. Then, the whole concerned frequency range is divided into multiple frequency ones. In each frequency range, 2~3 modes of composite thin plate are included. Finally, the iteration calculation techniques are employed to construct the frequency relative error function e_{fre} between the experimental and the theoretical natural frequencies in each frequency range, which is expressed as the following form

$$e_{\text{fre}} = \sum_{i=1}^{R_m} \left(\frac{|\Delta f_i|}{\hat{f}_i} \right)^2 \quad (36)$$

where R_m represents the number of modes in the whole frequency range, Δf_i represents the difference between the i th natural frequency obtained by the experiment and theoretical calculation, \hat{f}_i is the i th natural frequency obtained by the experiment.

By taking the elastic coefficients at normal temperature as the center, such as $E_1^0, E_2^0, G_{12}^0, \nu_{12}^0$, and with the consideration of parameters error $R_{\text{err}}=50\%$ caused by the temperature change, the range of these material parameters under certain temperature condition can be determined as the follows.

$$\begin{aligned} E_1^0 (1 - R_{\text{err}}) &\leq E_1' \leq E_1^0 (1 + R_{\text{err}}) \\ E_2^0 (1 - R_{\text{err}}) &\leq E_2' \leq E_2^0 (1 + R_{\text{err}}) \\ G_{12}^0 (1 - R_{\text{err}}) &\leq G_{12}' \leq G_{12}^0 (1 + R_{\text{err}}) \\ \nu_{12}^0 (1 - R_{\text{err}}) &\leq \nu_{12}' \leq \nu_{12}^0 (1 + R_{\text{err}}) \end{aligned} \quad (37)$$

Further, select an appropriate step size g (for example $g=1\%$) in the above range, and construct the

iteration vectors of elastic coefficients, such as $E'_1, E'_2, G'_{12}, \nu'_{12}$ under certain temperature condition, which can be expressed as

$$\begin{aligned} \mathbf{E}'_1 &= [E_1'^1 \ E_1'^2 \ E_1'^3 \ \cdots \ E_1'^n] \\ \mathbf{E}'_2 &= [E_2'^1 \ E_2'^2 \ E_2'^3 \ \cdots \ E_2'^n] \\ \mathbf{G}'_{12} &= [G_{12}'^1 \ G_{12}'^2 \ G_{12}'^3 \ \cdots \ G_{12}'^n] \\ \mathbf{\nu}'_{12} &= [\nu_{12}'^1 \ \nu_{12}'^2 \ \nu_{12}'^3 \ \cdots \ \nu_{12}'^n] \end{aligned} \quad (38)$$

By iteratively calculating these elastic coefficients in a permutation and combination manner, the values of $E'_1, E'_2, G'_{12}, \nu'_{12}$ under a certain temperature condition can be obtained when the frequency relative error function e_{fre} reaches the minimum value.

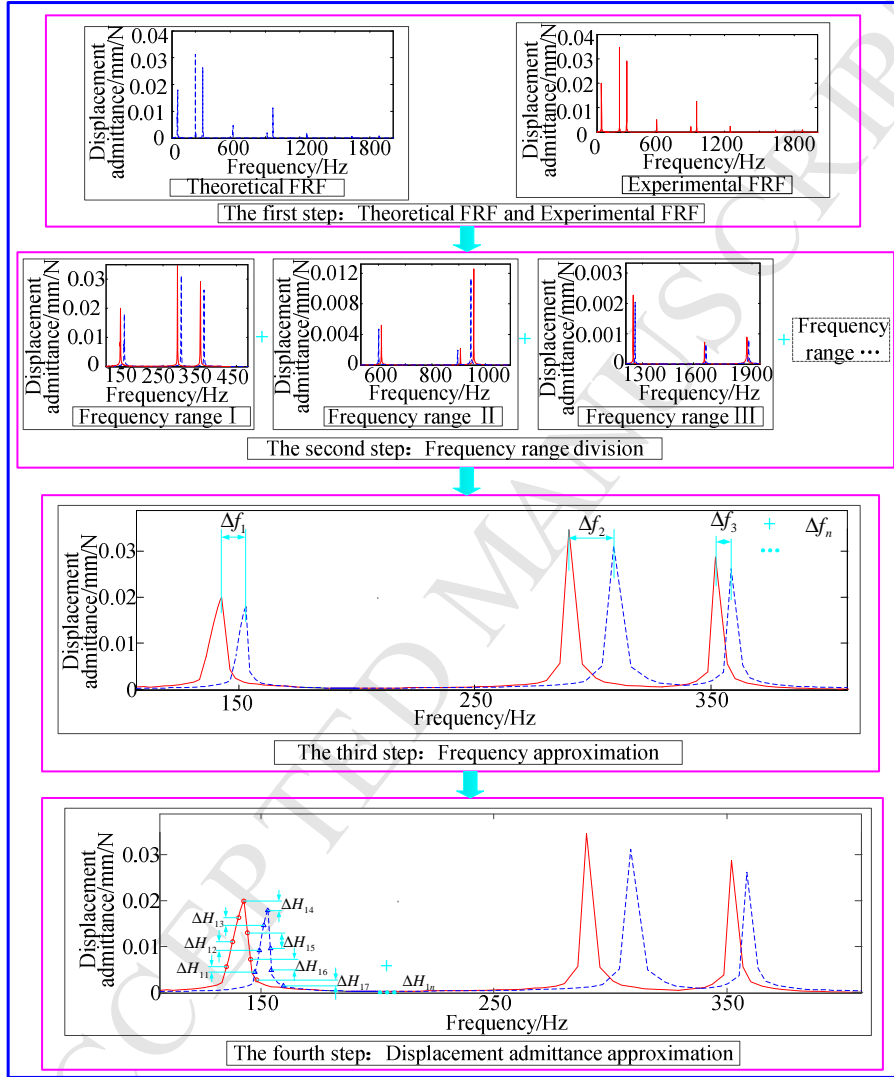


Fig. 3 The identification schematic of material parameters of fiber-reinforced composite in thermal environment

Similarly, by extracting the multiple resonant peaks from the experimental FRF data and the theoretical FRF data, the admittance relative error function e_{rec} can be obtained, which has the following form

$$e_{\text{rec}} = \sum_{r=1}^{S_m} \left(\frac{|\Delta H_{ir}|}{|\hat{H}_{ir}|} \right)^2 \quad (39)$$

where S_m is the number of approximation points on the i th resonant peak, $|\hat{H}_{ir}|$ represents the amplitude of the i th experimental FRF at the approximation point r ,

$|\Delta H_{ir}|$ represents the difference of amplitude between the i th experimental FRF and theoretical FRF.

Next, assume the maximum loss factor $\eta = 0.04$ and construct the iteration vectors of loss factors, such as $\boldsymbol{\eta}_1, \boldsymbol{\eta}_2$ and $\boldsymbol{\eta}_{12}$ with an appropriate step size g (for example $g=1\%$) in a range of $0 \sim \eta$, which can be expressed as

$$\begin{aligned} \boldsymbol{\eta}_1 &= [\eta_1^1 \ \eta_1^2 \ \cdots \ \eta_1^n] \\ \boldsymbol{\eta}_2 &= [\eta_2^1 \ \eta_2^2 \ \cdots \ \eta_2^n] \\ \boldsymbol{\eta}_{12} &= [\eta_{12}^1 \ \eta_{12}^2 \ \cdots \ \eta_{12}^n] \end{aligned} \quad (40)$$

where $\eta_{ij}^1 = 0, \eta_{ij}^2 = g\eta, \dots, \eta_{ij}^n = (n-1)g\eta$.

By iteratively calculating the loss factors in a permutation and combination manner, the values $\eta'_1, \eta'_2, \eta'_{12}$ under certain temperature conditions can be obtained when the admittance relative error function e_{rec} gets to the minimum value. Finally, by repeating the above process, the material parameters $E'_1, E'_2, G'_{12}, \nu'_{12}, \eta'_1, \eta'_2, \eta'_{12}$ under different temperature conditions can be obtained. It should be noted that the FRF approximation method can also be used to obtain the material parameters under normal temperature, such as $E_1^0, E_2^0, G_{12}^0, \nu_{12}^0, \eta_1^0, \eta_2^0, \eta_{12}^0$, as long as the experimental FRF result is obtained. It is suggested that the FRF measurements under normal temperature should be made by the hammer excitation, since it is more convenient and faster than the excitation of force sensor driven by the aerodynamic load.

3.3 Determination of the fitting coefficients

Once the material parameters of fiber-reinforced composite under different temperature conditions as well

as normal condition have been determined. Further, by choosing the temperature change ΔT as the independent variable, and the elastic moduli, Poisson's ratios and loss factors along different fiber directions as the dependent variables respectively, the concerned fitting coefficients, such as $A_n, B_n, C_n, D_n, F_n, H_n$ and P_n , can be determined by the curve fitting technique. In this way, the unknown coefficients in the Eq. (1) are obtained completely, which reflects the influence of the high temperature on the fiber-reinforced composite. By referring to the conclusions in the literature [27-29], the cube of ΔT is accurate enough to determine the fitting coefficients. So, the corresponding maximum value of the polynomial order in Eq. (1) is recommended as $n_0 = 3$. When all the predetermined coefficients are obtained, the natural characteristics, dynamic response and damping behaviors with considering the temperature dependent property can be predicted and analyzed. The analysis flow of the nonlinear dynamic characteristics of FCTP in thermal environment can be seen in Fig. 4.

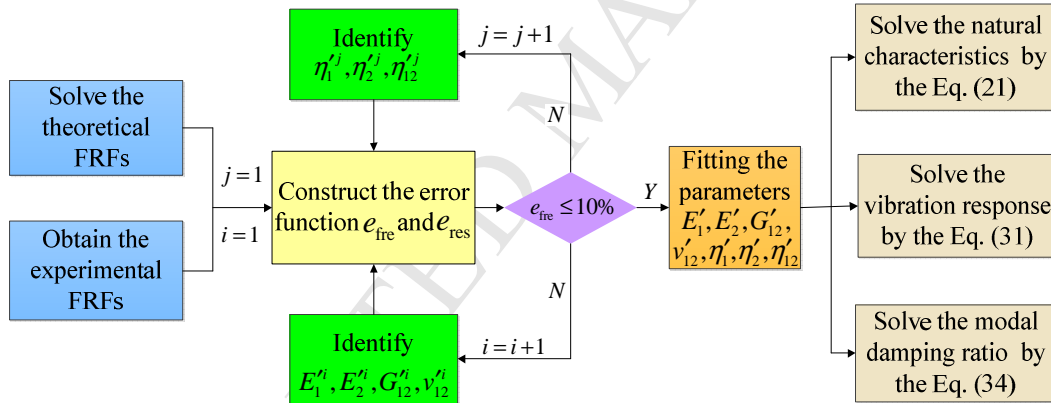


Fig. 4 The analysis flow of the nonlinear dynamic characteristics of FCTP in thermal environment

4. A case study

In this section, a TC500 carbon/epoxy composite thin plate was made to carry out a case study. Its nonlinear natural frequency, dynamic response and damping results were measured under different temperature conditions, which were used to verify the practicability and reliability of the established nonlinear model of FCTP in thermal environment.

4.1 Test object and test system

The TC500 carbon/epoxy composite thin plate was symmetrically laid, made by Jiangxi Jiujiang Diwei composite materials Co.Ltd. It has total 21 layers with laminate configuration of $[(0^\circ/90^\circ)_5/0^\circ/(90^\circ/0^\circ)_5]$, and each layer has the same thickness and fiber volume fraction with longitudinal elastic modulus of 132GPa,

transverse elastic modulus of 7.92GPa, shear modulus of 5.28GPa, Poisson's ratio of 0.32 and density of 1780kg/m^3 under normal temperature. The thermal expansion coefficients parallel and perpendicular to the fiber direction are $-0.15 \times 10^{-6}/^\circ\text{C}$ and $1.3 \times 10^{-6}/^\circ\text{C}$ respectively.

In order to ensure the experimental reliability in thermal environment, three composite thin plates with the same material parameters yet different sizes, namely composite plate A, B and C, were used in the test, as shown in Fig. 5. The length, width and thickness of them were $260\text{mm} \times 175\text{mm} \times 2.36\text{mm}$, $155\text{mm} \times 90\text{mm} \times 2.36\text{mm}$ and $230\text{mm} \times 130\text{mm} \times 2.36\text{mm}$, respectively. Then, the vibration test system in thermal environment was set up,

as shown in Fig. 6, to measure the nonlinear natural frequencies, modal shapes, dynamic responses and damping parameters of the plates. In the experiment, the clamp fixture and M8 bolts were used to clamp the plate specimens firmly to simulate the cantilever boundary condition. The laser measuring point was 60mm above

the constraint end, while the horizontal distance between this point and the left free edge of the three plates was 20mm. Also, the excitation point was located at about 2/3 of the length of the three plates above the constraint end, while the horizontal distance between this point and the right free edge was 20mm.

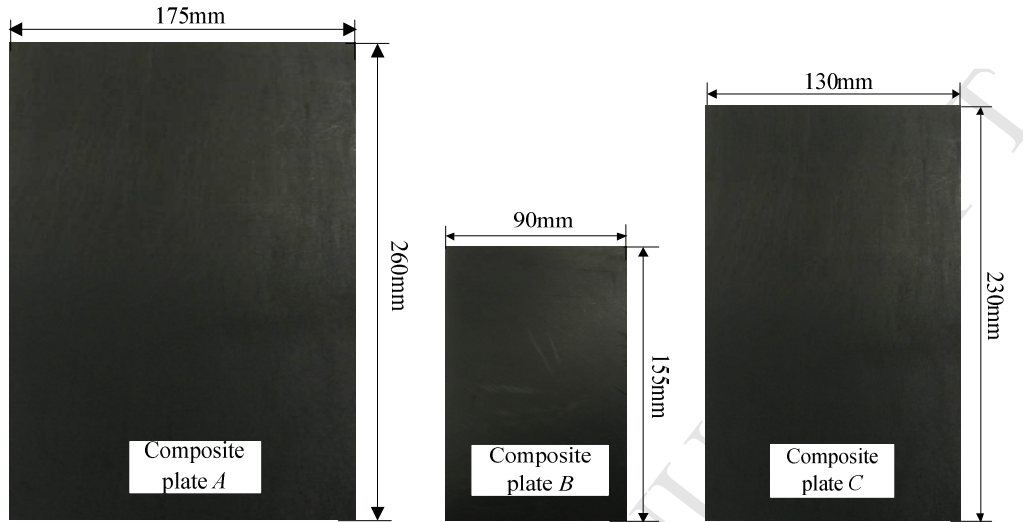


Fig. 5 The three different TC500 carbon/epoxy composite thin plates

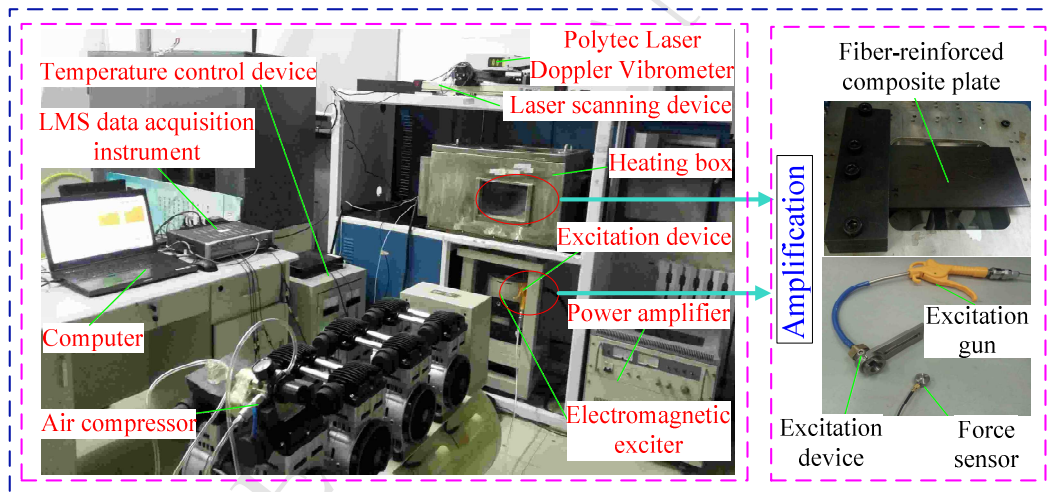


Fig. 6 Test system of FCTP in thermal environment

The instruments used in the test system were as follow: (I) Lianneng JZK-100 electromagnetic exciter and YE5878 power amplifier; (II) Lianneng force sensor CL-YD-301; (III) OTS 1500x4-160L air compressor (IV) Polytec PDV-100 laser Doppler vibrometer; (V) Two-dimensional laser scanning device based on LabVIEW control software; Yongyang PT100 thermocouple; (VI) Changbai Heating box T-500 and temperature control device C-500; (VII) LMS SCADAS 16-channel data acquisition instrument and Dell notebook computer (with Intel Core i7 2.93 GHz processor and 8G RAM to operate LMS Test.Lab 10B software).

In the test set-up, the heating box was used to provide the required temperature, and there was a high

temperature glass on the top of the box (Fig. 6), so that the laser Doppler vibrometer could be used to measure the response signal of the plate specimens through penetrating the glass. Besides, the motion of laser point was powered by the two-dimensional laser scanning device controlled by LabVIEW software. Both the pulse excitation and base excitation in thermal temperature were used in the experiment, where the change of temperature degree was measured by two thermocouples (one was to measure the temperature value, the other was employed as the feedback signal to the temperature control device). For the pulse excitation load, the force sensor driven by the aerodynamic load, which was provided by the air compressor, was used to excite the

plate specimens. For the base excitation load, the electromagnetic exciter and power amplifier were used to produce vibration excitation energy to the plate. These vibration and temperature signals were all recorded and stored by LMS SCADAS 16-channel data acquisition instrument and the notebook computer.

4.2 Identification of the fitting coefficients in thermal environment

Based on the established test system in Fig. 6, the FRFs of FCTP in thermal environment were obtained, as shown in Fig. 7. Then, the FRFs can be calculated based on the theoretical model, and the results are also plotted in Fig. 7.

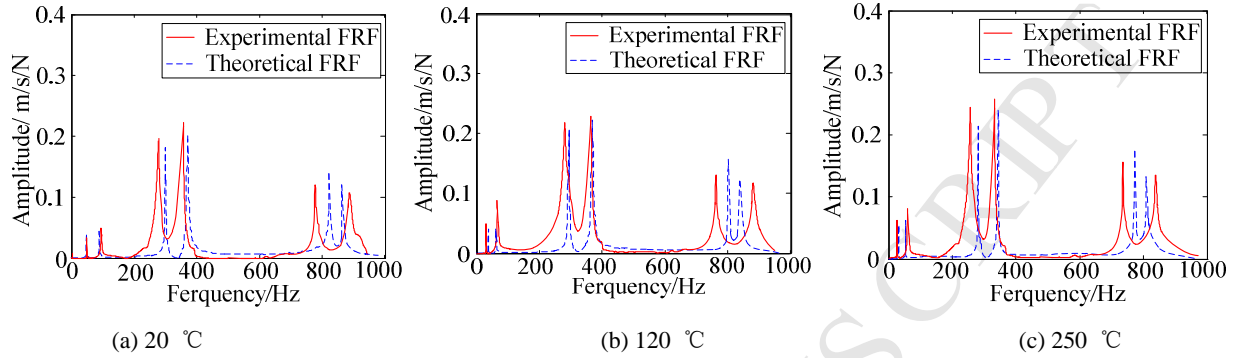


Fig. 7 The FRFs of FCTP under different temperatures

Next, using the FRF approximation method, the material parameters of the composite thin plates under different temperature environments can be identified. Table 1 shows the identified material parameter values of

both plate *A* and *B* at the following seven temperatures, i.e. 20 (normal temperature), 60, 80, 120, 160, 200 and 250°C

Table 1. The identified material parameter values of both *A* and *B* plates under different temperatures

Material parameters	Object	Temperature (°C)						
		20	60	80	120	160	200	250
E_1 (GPa)	Plate <i>A</i>	128.41	125.37	123.40	120.06	116.41	111.72	104.54
	Plate <i>B</i>	129.12	126.08	124.19	120.46	116.08	110.74	103.48
	Average	128.77	125.73	123.80	120.26	116.25	111.23	104.01
E_2 (GPa)	Plate <i>A</i>	8.08	7.91	7.68	7.39	7.04	6.45	5.68
	Plate <i>B</i>	8.13	7.82	7.54	7.32	6.96	6.30	5.56
	Average	8.11	7.87	7.61	7.36	7.00	6.38	5.62
G_{12} (GPa)	Plate <i>A</i>	5.40	5.23	5.12	4.95	4.76	4.53	4.11
	Plate <i>B</i>	5.48	5.28	5.19	5.03	4.80	4.49	4.08
	Average	5.44	5.26	5.16	4.99	4.78	4.51	4.10
ν_1	Plate <i>A</i>	0.332	0.331	0.330	0.331	0.330	0.333	0.332
	Plate <i>B</i>	0.334	0.332	0.329	0.330	0.330	0.331	0.333
	Average	0.333	0.332	0.330	0.331	0.330	0.332	0.333
η_1 (%)	Plate <i>A</i>	0.682	0.713	0.765	0.814	0.864	0.927	0.996
	Plate <i>B</i>	0.667	0.725	0.784	0.831	0.892	0.958	1.123
	Average	0.675	0.719	0.775	0.823	0.878	0.943	1.060
η_2 (%)	Plate <i>A</i>	0.793	0.821	0.864	0.912	1.027	1.145	1.312
	Plate <i>B</i>	0.765	0.806	0.853	0.936	1.083	1.177	1.296
	Average	0.779	0.814	0.859	0.924	1.055	1.161	1.304
η_{12} (%)	Plate <i>A</i>	0.855	0.958	1.036	1.124	1.257	1.413	1.602
	Plate <i>B</i>	0.883	0.956	1.051	1.153	1.295	1.406	1.624
	Average	0.869	0.957	1.044	1.139	1.276	1.410	1.613

It can be seen from Table 1, the change of Poisson's ratio ν_1 is very small as the temperature rise, and hence

the influence of temperature on the Poisson's ratio can be ignored. Then, the average results of composite material

parameters in Table 1 under different temperatures are brought into Eq. (1), and the concerned fitting coefficients of fiber-reinforced composite in thermal environment can be obtained as follows

$$\begin{aligned} E'_1(\Delta T) &= 128.77 - 7.795 \times 10^{-2}(\Delta T) - 2.44 \times 10^{-5}(\Delta T)^2 - 4.58 \times 10^{-7}(\Delta T)^3 \\ E'_2(\Delta T) &= 8.11 - 6.952 \times 10^{-3}(\Delta T) + 1.23 \times 10^{-6}(\Delta T)^2 - 7.965 \times 10^{-8}(\Delta T)^3 \\ G'_{12}(\Delta T) &= 5.44 - 4.767 \times 10^{-3}(\Delta T) + 7.55 \times 10^{-6}(\Delta T)^2 - 5.296 \times 10^{-8}(\Delta T)^3 \\ \eta'_{12}(\Delta T) &= 0.675 + 1.824 \times 10^{-3}(\Delta T) - 5.072 \times 10^{-3}(\Delta T)^2 + 1.976 \times 10^{-8}(\Delta T)^3 \\ \eta'_2(\Delta T) &= 0.779 + 2.569 \times 10^{-4}(\Delta T) + 1.597 \times 10^{-5}(\Delta T)^2 - 3.155 \times 10^{-8}(\Delta T)^3 \\ \eta'_1(\Delta T) &= 0.869 + 2.44 \times 10^{-3}(\Delta T) + 2.785 \times 10^{-6}(\Delta T)^2 + 2.833 \times 10^{-9}(\Delta T)^3 \end{aligned}$$

Fig. 8 and Fig. 9 show the fitted curves of the elastic moduli E'_1 , E'_2 , G'_{12} and loss factors η'_{12} , η'_2 , η'_1 under different temperatures when the cubic polynomial is employed. It can be seen that with the increase of

temperature, the elastic moduli of FCTP decrease in all directions, but the material loss factors show the increasing tendencies in different degrees (Fig. 9).

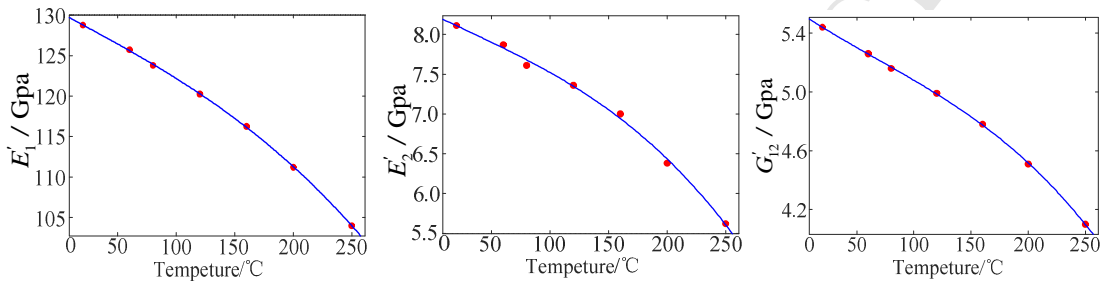


Fig. 8. The fitted curves of E'_1 , E'_2 and G'_{12} of fiber-reinforced composite under different temperatures

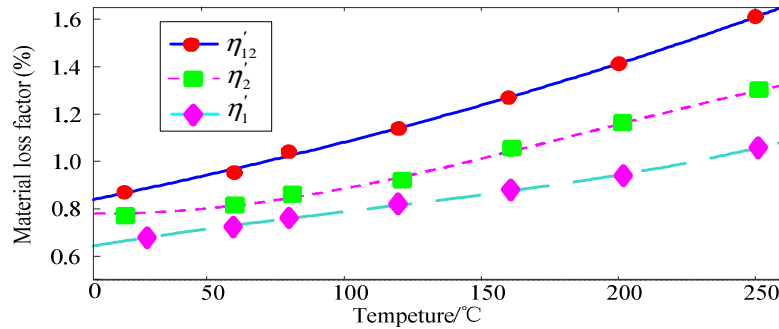


Fig. 9. The fitted curves of η'_{12} , η'_2 and η'_1 of fiber-reinforced composite under different temperatures

4.3 Comparison and verification of the inherent characteristics in different thermal environments

In order to verify the correctness of the theoretical model and study the effect of different temperatures on the dynamic characteristics of FCTP, the composite plate C was taken as the research object. By identifying the measured FRF results, the first 6 natural frequencies of the plate C are obtained at the temperatures of 20, 50, 100 and 200 °C, as shown in Table 2. Also, in order to study the effect of high temperature environment on the modal shapes of FCTP, the base excitation technique was employed in the established test system (Fig. 6) to excite the plate at different resonance state. Then, each modal shape in different thermal environments can be measured by the laser linear scanning method [30], as shown in

Table 3. It should be noted that the excitation levels used in this measurement need be controlled at the normal level, so as to avoid the overload phenomenon of laser Doppler vibrometer, and also to prevent the composite plate specimen producing large deformation, which will lead to the geometrically nonlinear vibration phenomenon.

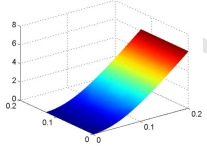
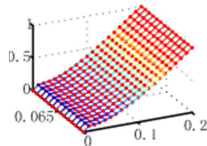
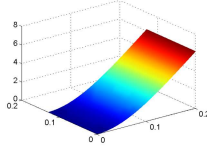
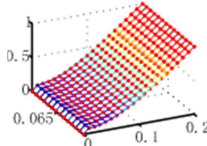
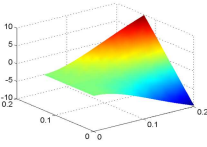
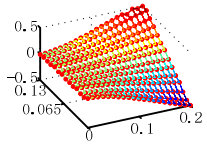
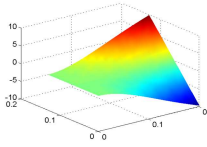
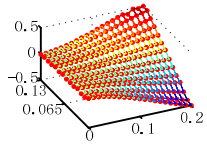
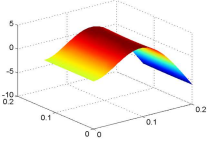
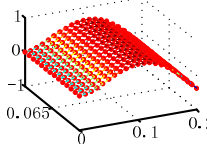
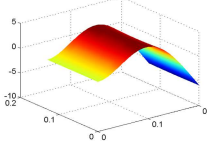
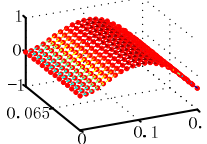
Finally, by substituting the material parameter values obtained from the fitting curves under different temperatures into the theoretical model, the corresponding natural frequencies and modal shapes with considering the temperature dependence can be calculated, which were also listed in Table 2 and Table 3. In addition, in order to compare the effects on the natural frequencies with and without considering the temperature

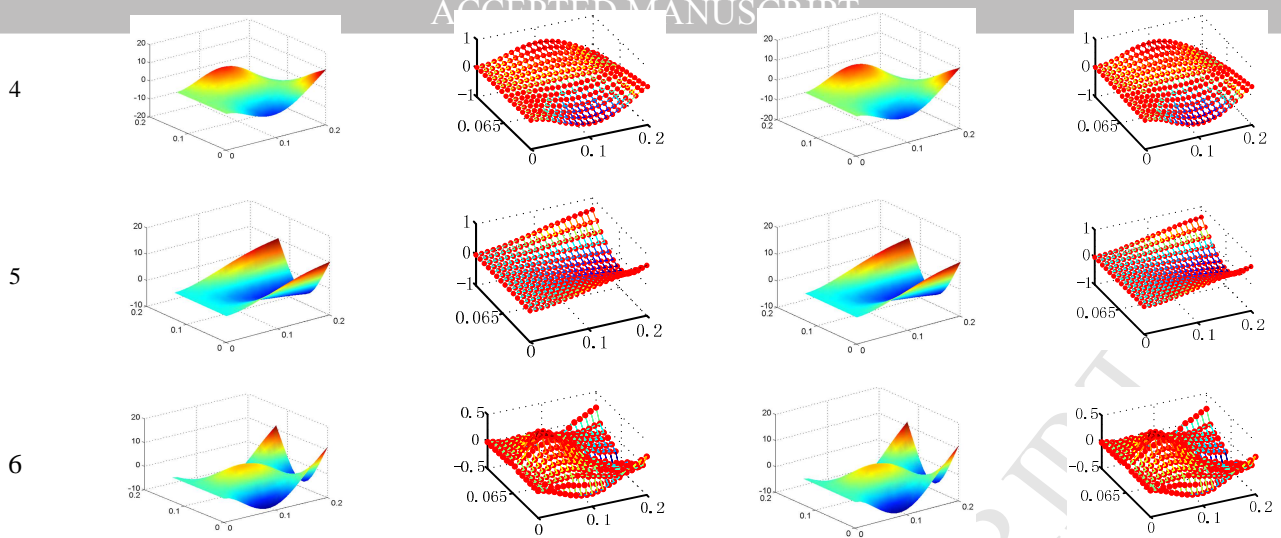
independence, the natural frequencies and the dependence were also given in Table 2. corresponding errors without considering the temperature

Table 2. The experimental and calculated natural frequencies of the composite plate *C* under different temperatures as well as the corresponding calculation errors with and without considering the temperature dependence

Temperature (°C)	Type	Modal order					
		1	2	3	4	5	6
20	Experimental test <i>A</i> /Hz	46.2	94.1	288.0	371.5	783.4	890.2
	Temperature dependence <i>B</i> /Hz	47.6	98.5	298.0	385.3	832.9	853.4
	Temperature independence <i>C</i> /Hz	47.6	98.5	298.0	385.3	832.9	853.4
	Errors (%) $ A-B /A$	3.0	4.7	3.4	3.7	6.3	4.1
	Errors (%) $ A-C /A$	3.0	4.7	3.4	3.7	6.3	4.1
50	Experimental test <i>A</i> /Hz	43.2	88.4	284.5	363.2	772.1	879.6
	Temperature dependence <i>B</i> /Hz	45.6	93.0	293.1	378.4	822.1	842.0
	Temperature independence <i>C</i> /Hz	46.20	94.51	296.83	383.74	832.73	852.70
	Errors (%) $ A-B /A$	5.6	5.2	3.0	4.2	6.5	4.3
	Errors (%) $ A-C /A$	6.9	6.9	4.3	5.6	7.8	3.0
100	Experimental test <i>A</i> /Hz	40.6	79.5	277.1	358.8	765.5	870.8
	Temperature dependence <i>B</i> /Hz	42.2	83.3	285.6	368.1	806.4	824.8
	Temperature independence <i>C</i> /Hz	44.0	88.5	292.1	378.8	828.5	847.8
	Errors (%) $ A-B /A$	3.9	4.8	3.1	2.6	5.3	5.3
	Errors (%) $ A-C /A$	8.3	11.3	5.4	5.5	8.2	2.6
200	Experimental test <i>A</i> /Hz	35.5	63.6	266.2	345.8	745.5	848.3
	Temperature dependence <i>B</i> /Hz	37.2	67.5	275.0	354.6	786.1	802.5
	Temperature independence <i>C</i> /Hz	38.5	71.3	289.2	373.5	825.0	844.5
	Errors (%) $ A-B /A$	4.8	6.1	3.3	2.5	5.4	5.4
	Errors (%) $ A-C /A$	8.5	12.1	8.6	8.0	10.7	4.5

Table 3. The experimental and calculated modal shapes of the composite plate *C* under different temperatures with considering the temperature dependence

Modal Order	Theoretical (20 °C)	Experimental (20 °C)	Theoretical (200 °C)	Experimental (200 °C)
1				
2				
3				



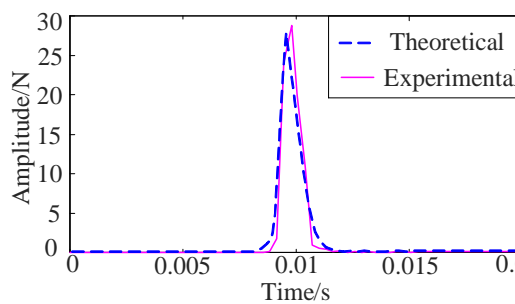
It can be seen from Table 2 and Table 3 that the thermal environment has a great influence on the natural frequencies of FCTP between the temperatures from 20 to 200 °C. The natural frequency results decrease with the increase of temperature, e.g., when the temperature is raised from 20 to 200 °C, the 1st and 2nd natural frequencies have the larger reduction rate compared with other modes. The calculated reduction rates are 21.8 % and 31.5% respectively, while the measured reduction rates are 23.2 % and 32.4 % respectively. This phenomenon is mainly due to the reduction in the elastic modulus and the structural stiffness matrix at high temperature. Moreover, there is a good agreement between the calculated and measured inherent characteristics, since the maximum calculation error of the first 6 natural frequencies with considering the temperature dependence is less than 6.5 %. From both theoretical and experimental results, it can be seen that the high temperature environment has little effect on the modal shapes of FCTP.

In addition, it can be seen from Table 2 that the natural frequencies of the composite thin plate calculated without considering the temperature dependence has a larger error compared with the experimental results

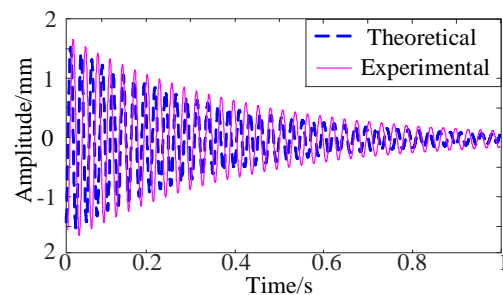
What's more, the higher the temperature, the greater the error. For example, when the temperature rises to 200°C, the maximum calculation error of the first 6 natural frequencies is 12.1%, yet the maximum error with considering the temperature dependence is 6.5%. Therefore, this nonlinear dynamic model can improve the calculation accuracy of natural frequencies (since it takes into account of the material nonlinearity induced by the high temperature).

4.4 Comparison and verification of the dynamic responses in different thermal environments

Here, the dynamic responses under the temperatures of 20, 50, 100 and 200 °C were measured when an impulse excitation was applied to the plate. The theoretical impulse responses were calculated based on the self-written MATLAB program. Taking 100 °C as an example, Fig. 10 shows the time-domain waveforms of the excitation signal and the response signal of the composite plate C. Fig. 11 shows the first 4 dynamic responses obtained from theoretical calculation and



(a) Excitation signal



(b) Response signal

Fig. 10 The time domain waveform of excitation signal and response signal under the temperature of 100 °C

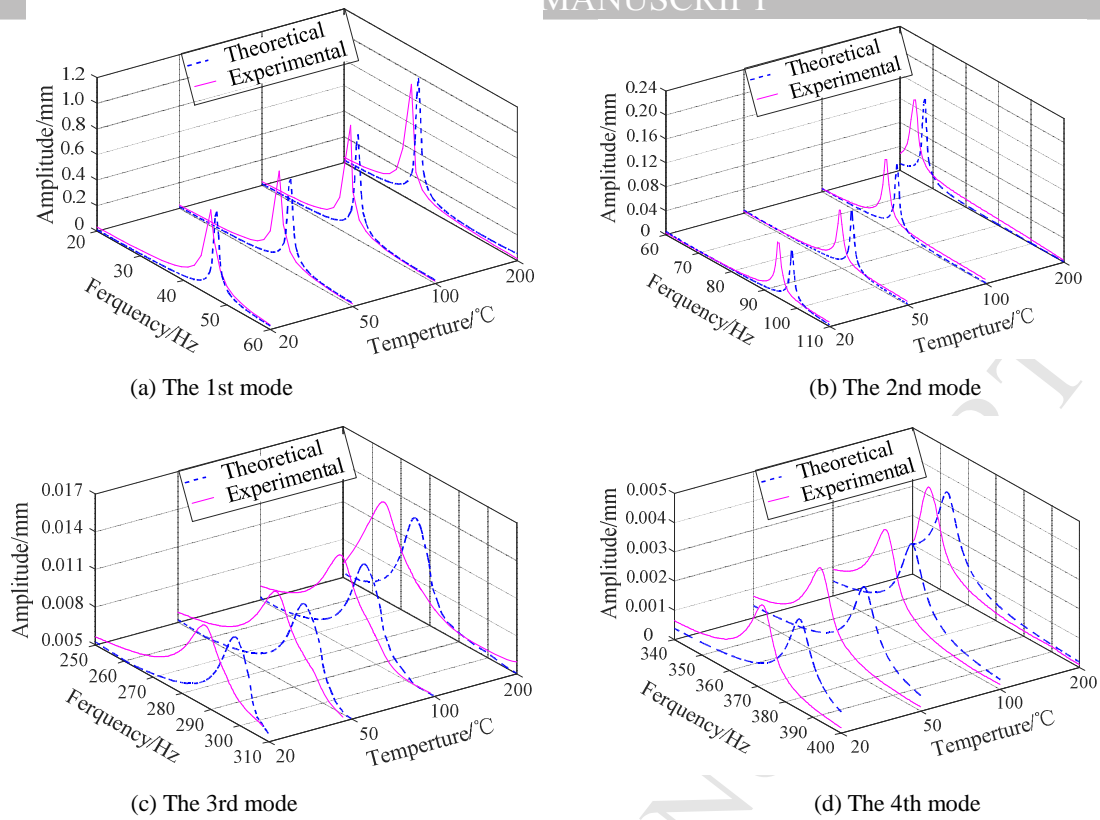


Fig. 11 The dynamic responses of the composite plate *C* obtained by theoretical calculation and experimental test under the temperature range of 20-200 °C

It can be seen from Fig. 11 that the dynamic response of FCTP increases with the rise of temperature, and the calculation errors under different thermal environments are within 9 %, which is within an acceptable range. The first dynamic response result is greatly affected by the temperature, e.g. the amplitude of the measured response increases from 0.68 mm at 20 °C to 0.92 mm at 200 °C, with an increase of 35.3 %. Besides, the measured response amplitudes in the 2nd, 3rd and 4th modes increase by 20, 13 and 12.3 %, respectively. From which we can see that with the increase of the mode order, the dynamic response of FCTP becomes increasingly insensitive to the high temperature. The reason for this nonlinear phenomenon may be that the first dynamic response is greatly affected

by the thermal expand stresses produced in the constraint end of FCTP, while the responses in the higher modes are comparably insensitive to the expansive deformation in thermal environment.

4.5 Comparison and verification of the damping results in different thermal environments

In this section, the first 6 modal damping ratios of the composite plate *C* under the temperatures of 20, 50, 100 and 200 °C were obtained by identifying the FRFs with the half power bandwidth method, as shown in Fig. 12. For the convenience of comparison, the calculated damping results and the corresponding scattergram of the composite plate *C* are also displayed in the same figure.

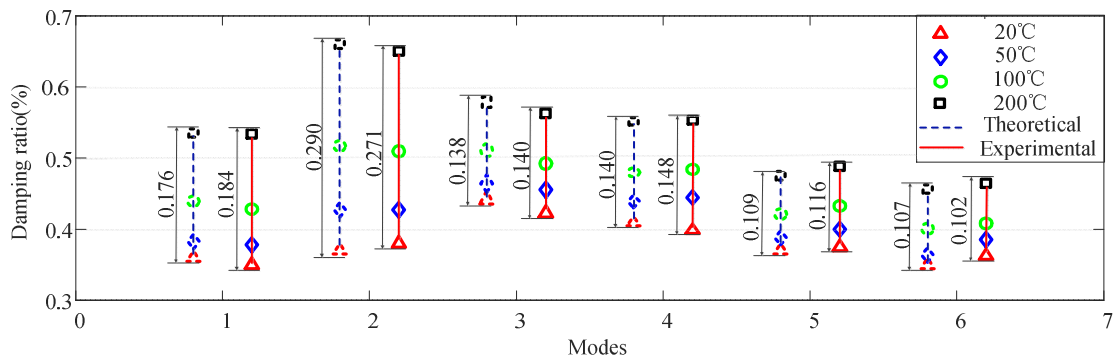


Fig. 12 The scattergram of the modal damping ratios of the composite plate *C* obtained by theoretical calculation and experimental test under

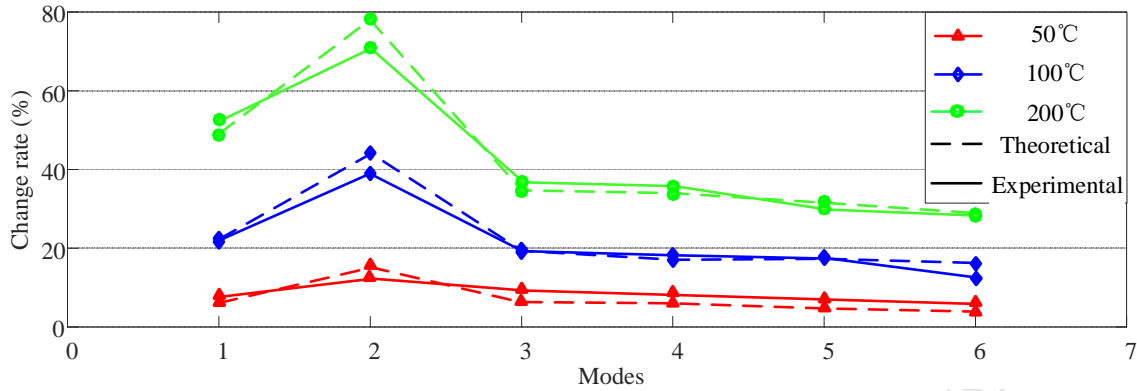


Fig. 13 The rising rate of modal damping ratios of the composite plate *C* at different temperatures obtained by theoretical calculation and experimental test

It can be seen from Fig. 12 that the increased thermal environment for the temperature range of 20-200 °C leads to a rise in each damping ratio of FCTP, with the errors of the calculated damping being within 5.6 % under different temperatures. In addition, the calculated rising rates in the first 6 damping ratios are 48.8, 78.4, 34.5, 33.6, 29.3 and 28.7 % respectively, while the measured rising rates are 52.6, 71.0, 36.9, 35.6, 30.1 and 28.1 % respectively. In order to visualize the effect of the increased temperatures on damping property, the rising rates of modal damping ratios of the composite plate *C* at 50, 100 and 200 °C are plotted in Fig. 13. From which we can see that the increased temperature has a greater effect on the damping characteristics in the lower modes of the composite plate, such as the 1st and 2nd damping ratios. However, high-order damping property of the composite thin plate seems to be insensitive to the increased temperature. For example, the increased levels of damping ratios in 5th and 6th modes are only about half that of the first 2 damping ratios. The reason for this maybe related with the energy dissipation capacity of interfacial friction in the composite plate. Because in high temperature environment, the microscopic interface friction phenomenon in the high-order vibration are not as violent as those in low-order vibration, which can be seen from high-order damping ratio results (they are lower than the first 2 damping ratios). Therefore, the increased temperature has less effect on high-order damping property.

Finally, it can be seen from the above results that the calculated errors on the natural frequencies, dynamic responses and modal damping ratios are less than 9%, which are quite reasonable. Also, the calculated modal shapes have a good agreement with the experimental

results, which validates the proposed nonlinear dynamic model of FCTP with temperature dependence in thermal environment.

5. Conclusions

In this paper, a nonlinear dynamic model of FCTP in thermal environment has been established, which is used to investigate the influence of thermal environment on the nonlinear dynamic characteristics of the composite thin plates. Based on the theoretical and experimental results, the following conclusions can be drawn:

(1) As the temperature increases, the elastic moduli of FCTP decrease in all directions, but the loss factors of the material show the increasing trends in different degrees.

(2) The natural frequencies of FCTP decrease with the increase of temperature. By taking the experimental results as an example, the measured natural frequencies in the first 6 modes decrease by 4.7 % - 32.4 % when the temperature is raised from 20 °C to 200 °C. However, the high temperature has little effect on the modal shapes.

(3) The dynamic responses of FCTP increase with the increase of temperature, especially the first vibration response results with the largest rising about 35%. However, with the increase of the mode order, the response becomes increasingly insensitive to the high temperature.

(4) The temperature contributes a rise in each damping ratio of the composite thin plate. However, high-order damping property of the composite thin plate seems to be insensitive to the increased temperature.

Acknowledgment

This study was supported by the National Natural Science Foundation of China granted No. 51505070, the

Fundamental Research Funds for the Central Universities of China granted No. N150304011, N160313002 N160312001 and N170302001, the Scholarship Fund of China Scholarship Council (CSC) granted No. 201806085032, and the Key Laboratory of Vibration and Control of Aero-Propulsion System Ministry of Education, Northeastern University, granted No.VCAME201603.

Declaration of Conflicting interests

The authors declared no potential conflicts of interest with respect to the research, authorship, and/or publication of this article.

References

- [1] Vinson J R, Sierakowski R L. The behavior of structures composed of composite materials[M]. Heidelberg: Springer Science & Business Media, 2006.
- [2] Jones R M. Mechanics of composite materials[M]. Washington: Scripta Book Company, 1975.
- [3] Reddy J N. Mechanics of laminated composite plates and shells: theory and analysis[M]. Florida: CRC press, 2004.
- [4] Rao B N, Pillai S R R. Non-linear vibrations of a simply supported rectangular antisymmetric cross-ply plate with immovable edges[J]. *Journal of Sound & Vibration*, 1992, 152(3):568-572.
- [5] Singh G, Rao G V, Iyengar N G R. Non-linear forced vibrations of antisymmetric rectangular cross-ply plates[J]. *Composite Structures*, 1992, 20(3):185-194.
- [6] Ribeiro P, Petyt M. Non-linear vibration of composite laminated plates by the hierarchical finite element method[J]. *Composite Structures*, 1999, 46(3):197-208.
- [7] Chen J, Dawe D J, Wang S. Nonlinear transient analysis of rectangular composite laminated plates[J]. *Composite Structures*, 2000, 49(2): 129-139.
- [8] Singha M K, Daripa R. Nonlinear vibration and dynamic stability analysis of composite plates[J]. *Journal of Sound & Vibration*, 2009, 328(4):541-554.
- [9] Whitney J M, Ashton J E. Effect of environment on the elastic response of layered composite plates[J]. *AIAA Journal*, 1971, 9(9): 1708-1713.
- [10] Ram K S S, Sinha P K. Hygrothermal effects on the free vibration of laminated composite plates[J]. *Journal of Sound & Vibration*, 1992, 158(1):133-148.
- [11] Gilat R, Aboudi J. Thermomechanical coupling effects on the dynamic inelastic response and buckling of metal matrix composite infinitely wide plates[J]. *Composite structures*, 1996, 35(1): 49-63.
- [12] Matsunaga H. Free vibration and stability of angle-ply laminated composite and sandwich plates under thermal loading[J]. *Composite Structures*, 2007, 77(2):249-262.
- [13] Li, W., & Li, Y. Vibration and sound radiation of an asymmetric laminated plate in thermal environments. [J]. *Acta Mechanica Solida Sinica*, 2015, 28(1):11-22.
- [14] Melo J D D, Radford D W. Time and temperature dependence of the viscoelastic properties of CFRP by dynamic mechanical analysis[J]. *Composite Structures*, 2005, 70(2):240-253.
- [15] YANG H Z, LI H J. Experimental modal analysis of the composite laminates with temperature variation[J]. *Acta Materiae Compositae Sinica*, 2008, 2(2):149-155.
- [16] Sefrani Y, Berthelot J M. Temperature effect on the damping properties of unidirectional glass fibre composites[J]. *Composites Part B: Engineering*, 2006, 37(4): 346-355.
- [17] Wu D, Wang Y, Shang L, et al. Experimental and computational investigations of thermal modal parameters for a plate-structure under 1200° C high temperature environment[J]. *Measurement*, 2016, 94: 80-91.
- [18] Praveen G N, Reddy J N. Nonlinear transient thermoelastic analysis of functionally graded ceramic-metal plates[J]. *International Journal of Solids and Structures*, 1998, 35(33): 4457-4476.
- [19] Duc N D, Thang P T, Dao N T, et al. Nonlinear buckling of higher deformable S-FGM thick circular cylindrical shells with metal–ceramic–metal layers surrounded on elastic foundations in thermal environment[J]. *Composite Structures*, 2015, 121:134-141.
- [20] Duc N D, Tuan N D, Tran P, et al. Nonlinear dynamic analysis of Sigmoid functionally graded circular cylindrical shells on elastic foundations using the third order shear deformation theory in thermal environments[J]. *International Journal of Mechanical Sciences*, 2015, 101-102:338-348.
- [21] Duc N D. Nonlinear thermal dynamic analysis of eccentrically stiffened S-FGM circular cylindrical shells surrounded on elastic foundations using the Reddy's third-order shear deformation shell theory[J]. *European Journal of Mechanics*, 2016, 58:10-30.
- [22] Duc N D, Nguyen P D, Khoa N D. Nonlinear dynamic analysis and vibration of eccentrically stiffened S-FGM elliptical cylindrical shells surrounded on elastic foundations in thermal environments[J]. *Thin-Walled Structures*, 2017, 117:178-189.
- [23] Duc N D, Kim S E, Chan D Q. Thermal buckling analysis of FGM sandwich truncated conical shells reinforced by FGM stiffeners resting on elastic foundations using FSDT[J]. *Journal of Thermal Stresses* 2018, 41(3):331-365.
- [24] Wang Y Q, Zu J W. Nonlinear dynamic thermoelastic response of rectangular FGM plates with longitudinal

- velocity[J]. *Composites Part B: Engineering*, 2017, 117: 74-88.
- [25] Gao K, Gao W, Wu D, et al. Nonlinear dynamic characteristics and stability of composite orthotropic plate on elastic foundation under thermal environment[J]. *Composite Structures*, 2017, 168: 619-632.
- [26] Thanh N V, Quang V D, Khoa N D, et al. Nonlinear dynamic response and vibration of FG CNTRC shear deformable circular cylindrical shell with temperature-dependent material properties and surrounded on elastic foundations[J]. *Journal of Sandwich Structures & Materials*, 2018:109963621775224.
- [27] Shen H S, Xiang Y, Lin F. Thermal buckling and postbuckling of functionally graded graphene-reinforced composite laminated plates resting on elastic foundations[J]. *Thin-Walled Structures*, 2017, 118: 229-237.
- [28] Nikrad S F, Asadi H. Thermal postbuckling analysis of temperature dependent delaminated composite plates[J]. *Thin-Walled Structures*, 2015, 97: 296-307.
- [29] Manalo A, Maranan G, Sharma S, et al. Temperature-sensitive mechanical properties of GFRP composites in longitudinal and transverse directions: A comparative study[J]. *Composite Structures*, 2017, 173: 255-267.
- [30] Li H, Chang Y, Xu Z H, et al. Modal shape measurement of fiber-reinforced composite plate with high efficiency and precision based on laser linear scanning method[J]. *Measurement and Control*, 2018, (accepted and will be published in the next 3 months)